MARTA Electronics Optimization

Rafaela Gramata[1,a]

[1] *Instituto Superior Técnico, Lisboa, Portugal*

Project supervisor: Pedro Assis

November 23, 2023

Abstract. Cosmic rays are still the focus of many experiments well after their first discovery. One of these experiments is the Pierre Auger Observatory, in which cosmic rays are detected through various methods. The observatory has been upgraded throughout the years with multiple new projects, one of which is MARTA, a project developed in order to better the knowledge of high-energy cosmic rays and their composition. This paper presents a study done on a DAQ board of MARTA to determine problems within and improve its performance. Several tests on the multiple functionalities of the acquisition software were performed to conclude about its efficiency. These experimentations show that the charge measurement, apart from the expected fluctuations, remains constant through different rates of triggers. However, the efficiency of trigger detection is optimal only for the lower rates. In one of the functionalities, "rate", a bug was found alongside its explanation.

KEYWORDS: MARTA, DAQ board, Pierre Auger Observatory, RPC detectors, Electronics

1 Introduction

1.1 Cosmic rays

Cosmic rays are tremendously energetic particles that propagate throughout space. These particles are nuclei produced in some of the most violent events in the universe. Once they come into collision with the atmosphere of Earth, they interact with its particles, creating extensive air showers, which are the cascades of particles obtained as an outcome of said collisions.

There are two methods of detection of cosmic rays: direct and indirect. The first employs balloons or satellite-borne detectors, while the second measures the air showers. Overall, both complement each other. The direct technique is the most accurate. However, it is not possible to obtain sufficient statistics due to the space and weight restraints of the balloons and satellites. As a result, interactions of high-energy cosmic rays with the atmosphere are measured at ground level using different types of detectors such as radio, particles, and light, while low energy rays (10^{14} eV) are measured by the direct method.

1.2 The Pierre Auger Observatory

The Pierre Auger Observatory, located in Argentina and with a detection area of 3,000 km^2, is the leading cosmic ray observatory. Designed by the Pierre Auger Collaboration with the purpose of better understanding high-energy cosmic rays and their origin, it counted on the work of more than 500 physicists from about 100 institutions. The observatory's construction began in 2002 and ended in 2008. However, it has collected data since 2004, gaining detectors as they became functional until 2008.

The observatory, classified as a hybrid detector, consists of a surface detector as well as a fluorescent detector. The surface detector is composed of 1660 water-Cherenkov stations and the fluorescent one comprises four stations

with six telescopes each as seen in Figure 1. The amount of time that the detectors are active is different for each. The surface detector is always operative, while the fluorescent one only records the light produced in the atmosphere by air showers on dark moonless nights. However, the measurements taken from the fluorescent detector are still of great importance. By measuring hybrid events, there is a way to calibrate the surface detector. Hence, a way to obtain more precise values for the energy of the particles.
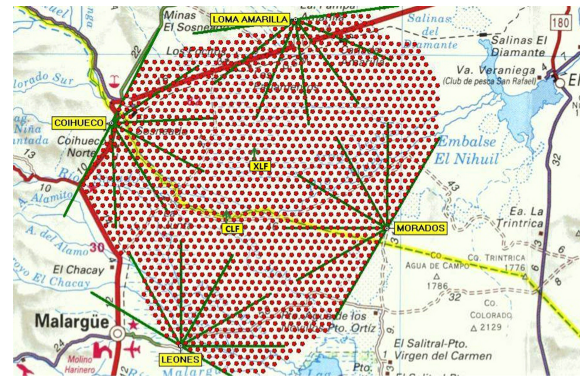
Figure 1. The Observatory: Each dot represents a surface detector station. There also are represented the 4 fluorescent stations along with each angle for its telescopes. Taken from [1].
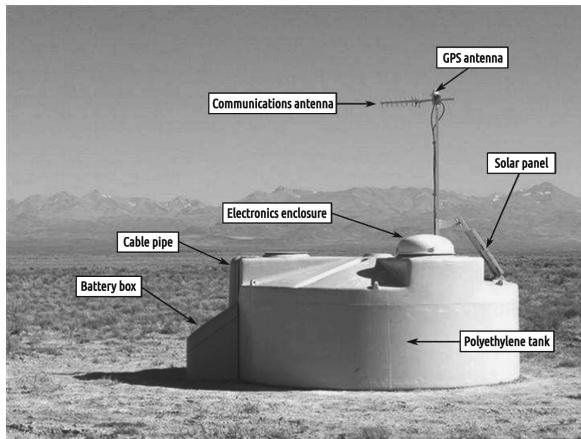
1.2.1 Detectors

1.2.1.1 Surface Detector

The surface detectors are cylindrical tanks filled with pure water that are able to measure Cherenkov light created by the movement of particles through the tank. The stations are self-powered by a solar power system, which supplies an average of 10 Watts for all the needed electronic components such as a GPS receiver, processor, radio transceiver and power controller alongside the photomultipliers, key elements to the process of detection of particles. These photomultipliers are in charge of recording the

---

[a]e-mail: rafaela.gramata@tecnico.ulisboa.pt

amount of light created in the tank, and all its produced signals are converted to digital signals by the DAQ system in place. Above these components, three hatches, covered with light- and water-tight hatch covers, give access to the interior of the tank. Their purpose is to enable people to fill the tank with water and install the interior parts. One of the hatches shelters the electronics in an aluminium dome that shuts out dust and rain. The electronics have a Tank Power Control Board that manages the power system and has the ability to hibernate the system in case of a low-charged battery.

Solar panels charge two 12 Volts batteries stored in a battery box insulated with foam to reduce high-temperature excursions throughout the day. This box is protected from direct sunlight in order to preserve the battery life through its installation on the shaded side of the tank. The solar panels, installed on aluminium brackets, support the mast, which, in turn, props up the antennas for communication and GPS. These antennas communicate with one of the four fluorescent stations, which in turn communicates with the central campus. This can all be seen in Figure 2.

Figure 2. Schematic view of a surface detector station along with its main components. Taken from [1].
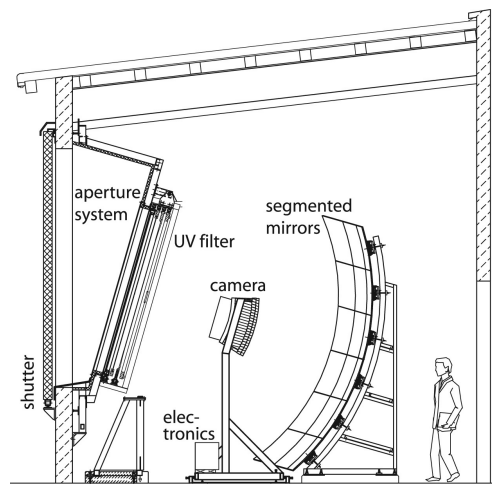
1.2.1.2   Fluorescent Detector

Figure 3. Fluorescent station along with its communication antenna. Taken from [2].

There are four stations of the fluorescent detector, each containing six ultraviolet telescopes in a controlled environment. Each of the six telescopes has a 30° field of view in azimuth. The stations combined create a 180° coverage, facing inwards, overlooking the surface detectors. In elevation, the telescopes also have a field of view of 30°. The telescopes, designed to measure air showers with an energy of 10^{18} eV [3], have Schmidt optics as a base for their design in order to reduce the coma aberrations of large optical systems.

The fluorescent light, emitted isotropically by the atmosphere after excitation by air showers, enters the station through a circular diaphragm embedded with a filter glass window. This filter lets through UV light, whereas visible light is unable to get past it. This way, background light reaching the camera is reduced. Moreover, it aids as a window over the aperture, keeping the climate clean and controlled in the room where the telescopes and the electronics are situated.

In Figure 4, we can see that shutters shelter the components. They are closed during the day and will automatically close at nighttime immediately after observing adverse weather conditions. Installed on the outer side of the aperture are corrector rings in order to rectify spherical aberration and remove the coma aberration. The light reaching the camera, previously focused by the segmented mirrors onto a spherical focal surface, is collected by hexagonal photomultiplier tubes.

Figure 4. Schematic view of a fluorescent detector and its components. Taken from [1]

1.3 MARTA

The project introduces a new concept of directly measuring muons in air showers. The acronym, Muon Array with RPCs for Tagging Air showers, explains that it employs resistive plate chambers, components that can detect charged particles with good time and space resolution.

It is designed as a hybrid detector concept, as it is to be associated with a water-Cherenkov tank (WCD). Crossing the data collected from the chambers with the data from a water-Cherenkov tank we can separate the muonic and

electromagnetic components of the air showers more efficiently. Thus, we can study the shower development more accurately.

Four resistive plate chambers are positioned under the water-Cherenkov tanks, which behave as a shield to the electromagnetic elements of the shower. The WCD is susceptive to both components, which improves the triggering efficiency. Moreover, the electrons and gammas of the shower are absorbed by the matter in the tank, making the muonic elements purer when reaching the chambers.
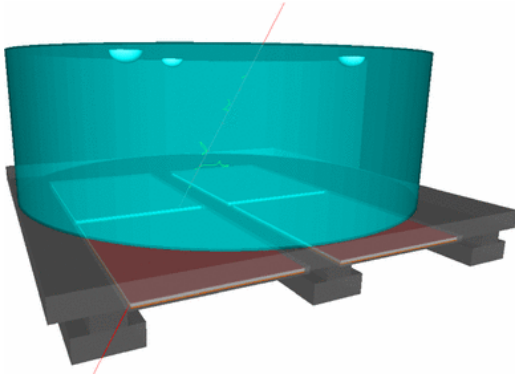

Figure 5. Illustration of a MARTA station. The RPCs (brown) under the Water Cherenkov tank (green). Taken from [4].

Since it is specifically designed to fit into a water-Cherenkov station, it takes advantage of the power, communications and trigger systems [5] of the surface detector it is associated with .

1.3.1 RPC detectors

Resistive Plate Chambers (RPC) are gaseous detectors known for being low-cost and efficient. The gas is contained by highly resistive parallel plates, on which it is induced high voltage. The high resistivity impedes electrical discharges, which could damage the detector. A strong and uniform electric field, created by the high voltage applied, produces avalanches of particles after initial ionization by the interaction of ionizing particles in the gas. When reaching the anode, a signal is induced in the readout electrodes.
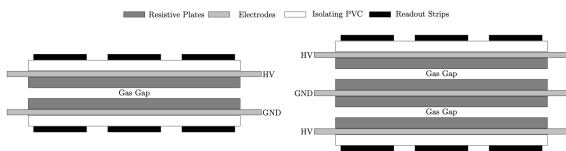

Figure 6. Schematic view of examples of a RPC. Taken from [3].

Environmental conditions highly influence the operation of gaseous detectors. Thus, it has always been thought that RPCs could only operate in laboratory circumstances. However, studies done in favour of MARTA's development

reveal otherwise [3]. They can function in severe conditions while maintaining their efficiency. Hence, being low-cost, they are a great addition to the project.

As shown in Figure 7, in a MARTA configuration, a subsystem is employed in the same aluminium shielding case as the RPCs. This system accommodates the high-voltage supplier, the gas monitoring bubbler block, the low-voltage supplier, the multiplexer and the communications.
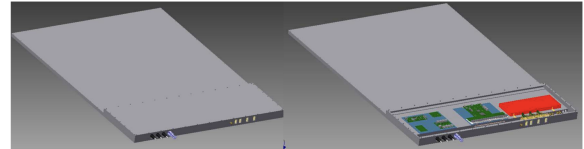
Figure 7. 3D CAD of the aluminium shielding box where the sensitive module and the pick up pad plane are assembled. The small extra volume will house the subsystems: HV power supply (red); gas monitoring bubbler block (yellow), MAROC front-end board (centre green board); LV power supply, multiplexer and gas system communication (left green boards). Taken from [6]

1.3.2 Electronics

Due to the space and energy limitations in the water-Cherenkov stations, all the electronics components require low energy consumption and small dimensions in order to fit into the aluminium box. With this in mind, they have developed boards for different purposes, such as the front-end, high voltage, power supply unit, Central Unit, etc. They are all present in Figure 8.

Figure 8. Boards developed to be used in MARTA. From top left to bottom right: front-end, high voltage, power supply unit, Central Unit, gas flux monitoring, I2C multiplexer, gas monitoring interface and gas pressure sensor. Taken from [5].

The front end reads the fast RPCs signals, making it the principal component in data acquisition. It is capable of reading the hits of the particles along with their charge. To execute these measurements, the board possesses a MAROC ASIC to digitize the signals. The MAROC meets all the space and energy requirements [3] while having 64 input channels, which is compatible with the data from the 8 x 8 grid of the RPCs. The ASIC digital outputs are input into an FPGA, which is in charge of the data, measurements and communications.

The way the MAROC works depends on the configurations supplied to it by an 828-bit file. In this file, we can customize the amplifier's gain, discriminator's thresholds and many more parameters.

When the signals enter the ASIC, they go through a pre-amplifier. Each of the 64 input signals have a pre-amplifier

with a gain correction from 0 to 4. Once amplified, the signals are copied to three branches: the fast shaper, the slow shaper and the sum branch.

The fast shaper is in charge of the discrimination of the signals. It produces fast signals with good time resolutions. The signal can go through one of three options of fast shapers, such as the unipolar, the bipolar and the half-bipolar. In MARTA, the chosen was the bipolar one due to the unfavourable characteristics of the others [3].

The slow shaper is behind the charge measurements. The amplified signal undergoes a variable RC circuit chased by a variable slow shaper. This way, a slow signal is created, from which the peak value is obtained. This value and the charge generated in the detector are known to be proportional. Once the signal is shaped, the baseline and peak are sampled by two sample and hold circuits. Two inputs of the ASIC, Hold1 and Hold2, common to all 64 channels and generated by the FPGA, determine the moment the signal is held. The signal then goes through a Wilkinson ADC of 12 bits to be digitized with increased resolution. The acquisition is interrupted when the signal reaches the communication process. Therefore, it creates dead time with a maximum of 13 ms [3] when in USB mode for the biggest data portion possible of transmission.
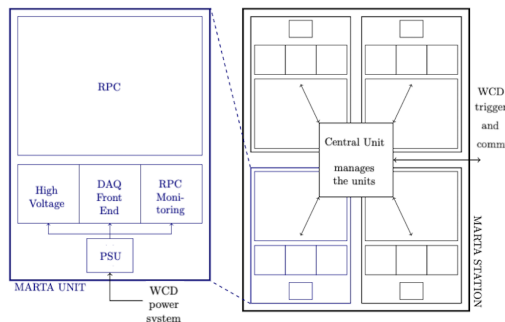
Figure 9. Diagram of a MARTA unit along with its electronics. Taken from [5].

As seen in Figure 9, the Central Unit is responsible for communicating with the water-Cherenkov detectors. Moreover, it controls all four elements in each MARTA station.

2 Experimental procedure

Given access to a DAQ board and a computer with the acquisition software installed, tests were performed on it in order to identify problems within. The Ctest, a test input configured to channel 63, can simulate an input charge through a 2 pF capacitor and was the primary method of inputting signals into the board.

The process began by understanding the code behind the data acquisition system, specifically, the charge measurement code. Once the command lines for measuring counts, charges and rates were found in the GitLab of the project, it was still a requirement to pinpoint the ones that were able to read the data collected. There were two folders

containing related information to the software, "ChargeScript" and "T-MARTA", the last being the same on Git-Lab mentioned earlier.

A charge measurement would create a .txt file in gray binary where each event corresponds to an 832-bit line, a count measurement would create a Root tree, and a rate measurement would generate a .txt file with the rate for each channel every minute.

It is thought that the "reading data" files on "T-MARTA" are supposed to work with the four units integrated into the MARTA station. Hence, too complex for the tests. Seeing the folder "ChargeScript", there was a way to read the files obtained in a charge measurement. The measurement would appear as a Root canvas of all 64 channels. Hence, it was adapted to only show the 63rd channel. To read the counts Tree, the only necessary action was to open it in Root. The only requirement to read the rate file was to open it because, as we know, during a whole minute, the rate function counts the triggers detected and then converts the counts per minute to counts per second, displaying it in a row for each channel.

To correctly measure anything, first, we need to send a command line of a measurement that sends the configuration file to the board, for example, a counts or charge measure. Otherwise, it will malfunction, for example, if you send a rate measure before anything else. Once the configuration file is sent, a LED (D13) will light up. All measurements were taken using the internal trigger of the board (OR trigger).

2.0.0.1 Experimental Apparatus
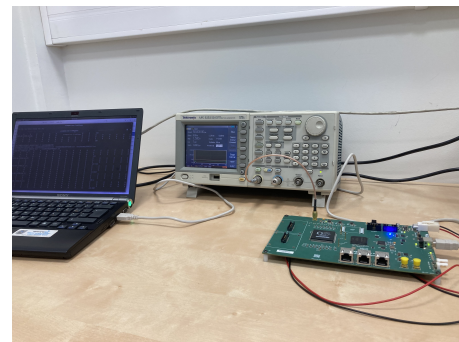
Figure 10. Equipment (from left to right): A computer with the acquisition system, a signal generator Tektronix AFG3252, a MARTA DAQ board and a power supply (out of the picture).

The board connected to the computer via USB receives 5 Volts from the power supply. The signal generator is connected to the CTest input and inputs square waves with amplitude proportional to the charge. In initial tests, a square wave signal found in the recall function was the one input. It had an amplitude of 1.5 V, a frequency of 8.5 Hz and 1 ms of delay.
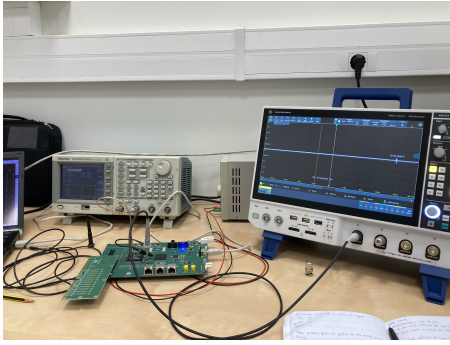
Figure 11. Equipment: Addition of a board that connects to channels and a oscilloscope.

Later, the square wave signal was changed, so its period wasn't larger than its delay, to a constant 50 μs. An input other than Ctest was also used. Connecting the signal generator to an actual channel of the board imitates the process in a MARTA unit. The channels used were 44 and 47. However, the cable appeared to have faulty contact, so it was no longer used. The oscilloscope seen in Figure 11 was used to ensure the correct passing of the signal through all the stages.

2.1 Counts

The count measurements, to find the maximum rate possible without ignoring triggers, were carried out for different set rates coming from the generator. The measure of the time taken to count 1000 events (specified in the command) was obtained from the Root tree. The measured rate versus the ideal rate is presented in Figure 12.
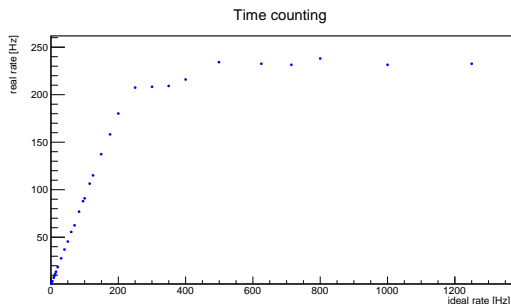
Figure 12. Graph of measured rate versus .

It was expected for the graph in Figure 12 to be linear up to a certain point, as the time between signals outsizes the time it takes to detect the trigger. For higher set rates the system is expected to respond with the maximum count number. The linearity can be seen in the graph of Figure 13.
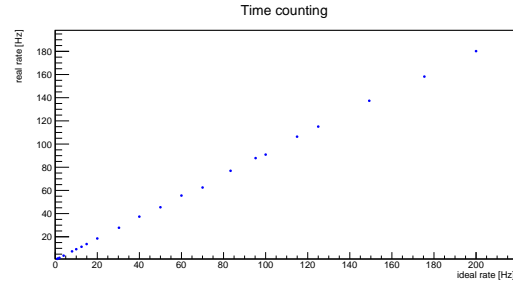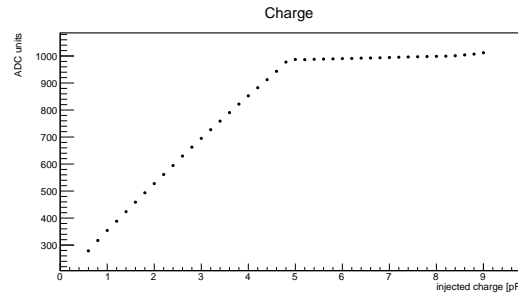

Figure 13. Graph illustrating the linearity in the lower range of rates.

A linear regime is found up to ≈ 200 Hz and then saturates with a response near 230 Hz.
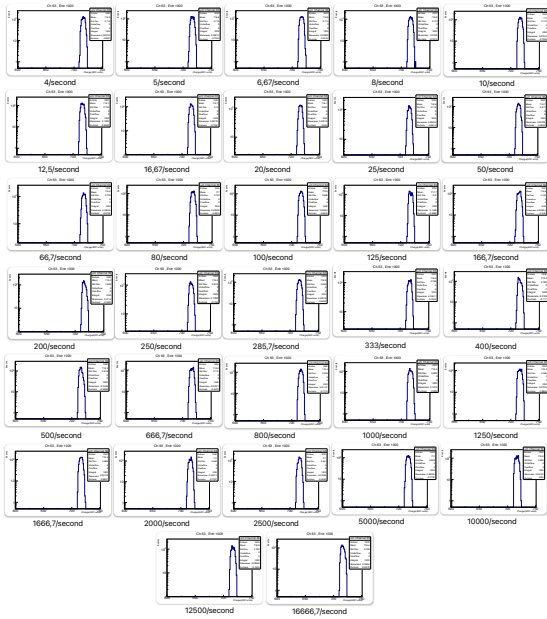
2.2 Charge

The charge measurements began with a sweep of voltages of the square wave in the signal generator, equivalent to different charges, to find the limit when the board no longer has a sensibility to a difference in charge. The graph in Figure 14 shows the measurement (in ADC units) related to the supposed charge calculated as $Q = CV$ in which Q is the charge, C the capacitance of the capacitor in Ctest and V the voltage of the signal for channel 63. This information is specific to channel 63 and not general to the whole board because, as seen in [3], the measurement of charge outputs different values for different channels.

Figure 14. Graph illustrating the range of charges that the board is sensible to.

It is noticeable that the board does not have sensibility to a difference in charge when the injected charge reaches 5 pF. There is a linear regime up to that point and it saturates past it.

For the rest of the measurements, the voltage was maintained at 1.5 Volts. Apart from quantifying charge, another significant aspect is how the measurement reacts to larger rates. It was expected that there would be a pileup of triggers or that the board would ignore most. Therefore, a graph illustrating this would either have the charge increasing with the rate for the first option or decreasing for the second. Each measure provides a charge distribution, meaning we can fit it into a Gaussian distribution and obtain the mean and standard deviation. These distributions can be seen in Figure 15.

Figure 15. Distributions of charge for different rates.

A graph containing the data from the mean and standard deviation is presented as well in Figure 16, which illustrates how the measure is unchanged past the expected fluctuations.
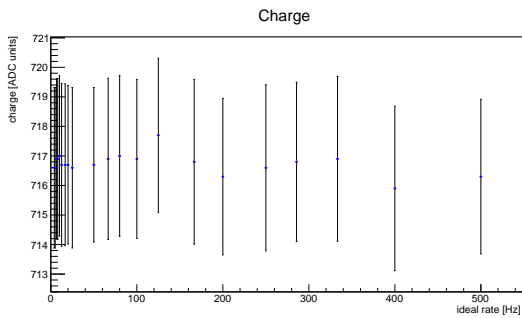

Figure 16. Graph comparing the obtained charge for each rate.

No change is noticeable in the distributions seen in Figure 15 other than the expected fluctuations, which shows that, at least, in this somewhat controlled environment, the rate is not affecting the measurement.

Another aspect we can look into is the time it takes to complete the measure. The graph in Figure 17 presents a comparison between the set rate and the real rate. It is noticeable that the values for the real rate are significantly smaller when compared to the counts' measurement. However, they are similar as both converge to a certain maximum rate. In the case of smaller rates, the linearity is still applied as an approximation, as seen in Figure 18.
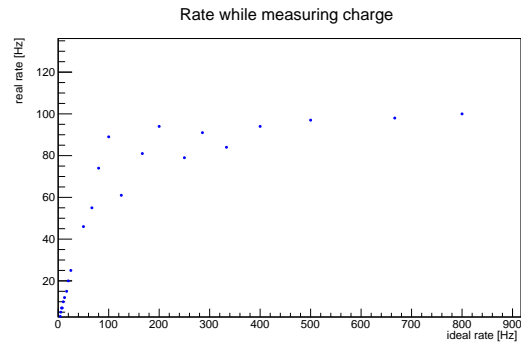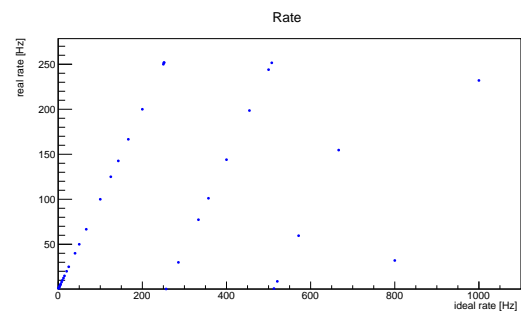

Figure 17. Graph illustrating the rate when measuring charge.
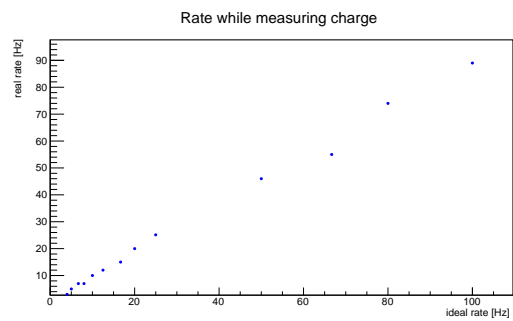
Figure 18. Graph illustrating the rate when measuring charge focused in smaller rates.

2.3 Rate

As mentioned before, the function of "rate" is to measure the number of triggers the board could detect for a whole minute and then convert it to rate per second. The running of the command first started as a way to make sure the signal was correctly passing through to the board. However, the results were far from the expected. Being correct for all the delay times larger than 3.9 ms, where it would take a value of a little over 256, to going back to "square one" and outputting around 0.4, it was a reason for concern. This can be seen in the graph of Figure 19.

Figure 19. Graph illustrating the bug found.

The problem was that in the acquisition code for the rate, the ADC is configured to 8 bits and not protected

against occasions in which the rate is larger than 256. Hence, the results obtained. This bug could be readily corrected by enlarging the register size in the Firmware.

3 Results and Conclusions

The main goals of this study were to determine problems and ways to better the DAQ boards of the MARTA project. The principal problem going into the study was thought to be the efficiency of trigger detection. However, in such a short time, there is difficulty in thoroughly understanding the inner workings of the board as well as improving them. This way, no improvements related to the principal problem mentioned before were made.

The research has shown that:

- In a counts measurement, the efficiency of the trigger detection is only maintained up to 200 or so counts per second.

- In a charge measurement, the charge remains the same throughout the rates measured, accounting for expected fluctuations. However, the efficiency of the detection of triggers is even worse than in a count measure, only staying approximately linear for the lower rates.

- In a rate measurement, a bug, leading to wrong results for the rate function, was found.

The problem related to the time it takes to detect specific amounts of triggers may be due to the ADC and the communication with the board, as they are the processes in which most time is spent after detection. One way to solve this would be to upgrade the ADC chosen to a more efficient one.

Acknowledgements

References

[1] T.P.A. Collaboration, Nuclear Instruments and Methods in Physics Research Section A: Accelerators, Spectrometers, Detectors and Associated Equipment **768** (2015)

[2] S. Saffi, *Pierre Auger Observatory Fluorescence Detector*, https://www.esa.int/ESA_Multimedia/Images/2021/12/Pierre_Auger_Observatory_Fluorescence_Detector (2021), [Online; Accessed in September 5, 2023]

[3] R.J.B. Luz, Ph.D. thesis, Universidade de Lisboa, Instituto Superior Técnico (2020)

[4] P. Abreu, S. Andringa, P. Assis, A. Blanco, V.B. Martins, P. Brogueira, N. Carolino, L. Cazon, M. Cerda, G. Cernicchiaro et al., The European Physical Journal C **78**, 333 (2018)

[5] P. Abreu, S. Andringa, P. Assis, A. Blanco, V.B. Martins, P. Brogueira, N. Carolino, L. Cazon, M. Cerda, G. Cernicchiaro et al., PoS **TWEPP2019** (2019)

[6] L. Lopes, A. Alves, P. Assis, A. Blanco, N. Carolino, M. Cerda, R. Conceição, O. Cunha, C. Dobrigkeit, M. Ferreira et al., Journal of Instrumentation **14**, C07002 (2019)